ELSEVIER

Journal of Alloys and Compounds 281 (1998) 56–59

Journal of ALLOYS AND COMPOUNDS

Studies on the structure and magnetic properties of $Sm_2(Fe,Al)_{17}C_Y$ alloys with Zr additions

Wei Tang[a,*], Jian-Ron Zhang[a], Zhi-Qiang Jin[a], Li-Ya Lu[a], You-Wei Du[a], Yan Wang[b], Jian-Jian Xu[b]

[a]*Department of Physics and National Laboratory of Solid State Microstructure, Nanjing University, Nanjing 210093, People's Repubic of China*

[b]*Institute of Applied Physics, Nanjing University, Nanjing 210093, People's Republic of China*

Abstract

The microstructure and magnetic properties of induction-melted and melt-spun $Sm_2(Fe,Al,Zr)_{17}C_Y$ samples with Zr additions have been systematically studied using X-ray diffraction, TEM, differential thermal analysis, and magnetic measurements. The results show that the induction-melted and melt-spun $Sm_2(Fe,Al,Zr)_{17}C_Y$ samples have a multi-phase structure with the 2:17-type carbide, α-Fe and ZrC phases. Both the Curie temperature and the lattice parameters of the 2:17-type structure are found to be almost constant with Zr addition but the saturation magnetization decreases with increasing Zr content. The addition of Zr is effective at eliminating α-Fe dendrites and preventing the precipitation of large size α-Fe phase through rapid quenching and annealing. The optimum coercivity of 11.6 kOe along with a remanence of 55 emu g^{-1} is obtained for a $Sm_2Fe_{15.3}Zr_{0.2}Al_{1.5}C_{1.5}$ ribbon spun at 40 m s^{-1} and annealed at 750°C for 30 min. It is presumed that the high remanence and coercivity are due to the small crystal size and significant exchange coupling at interphase boundaries.

Keywords: Magnetic properties; Melt-spinning; Microstructure; $Sm_2(Fe,Al,Zr)_{17}C_Y$; Zr addition

1. Introduction

Rare-earth–iron intermetallic compounds based on the 2:17 structure have been attracting much attention as potential permanent magnet materials since it was found that $Sm_2Fe_{17}C_Y$ compounds prepared by melt-spinning and substituting with other elements, such as Ga, Cr, Al, or Si for Fe [1–5], have improved magnetic properties and temperature stability. The substitution of Ga, Cr, Al for Fe in $Sm_2Fe_{17}C_Y$ compounds helps the formation of high carbon compounds with the 2:17-type structure. However, these compounds must have either a single phase with the 2:17-type structure or a nanoscale mixture of the 2:17-type and α-Fe phases to obtain high magnetic properties [5,6]. Recently, our research [7] showed that it is rather difficult to obtain a strong exchange coupling in a mixture of 2:17-type structure and α-Fe phases. When the mixture was melt-spun and then annealed, the α-Fe phase in the mixture readily became coarse and thus resulted in uncoupling to the hard magnetic phase. It was expected that the exchange coupling between the hard and soft magnetic phases could enhance remanence. Therefore, it was necessary to improve the microstructures further in order to obtain high remanence and coercivity. Along with other elements, Zr was introduced successfully into $Sm_2(Fe,Al,Zr)_{17}C_{1.5}$ alloys to improve both coercivity and remanence. In this paper, we report the detailed results of the Zr addition effects.

2. Experimental procedures

All the constituent elements of at least 99.8% purity were levitation-melted in a water-cooled copper crucible under an argon atmosphere to provide the starting ingots. An excess of 15% Sm was added to compensate for the evaporation loss of Sm during the melting and melt-spinning processes. The ingots were turned over and remelted four times to ensure homogeneity. The ingots were melt-spun in a standard melt-spinner under an argon atmosphere. The surface velocity of the Cu wheel was 40 m s^{-1}. The ribbons were then annealed under an argon atmosphere at 750°C for 15–60 min to crystallize and develop a fine microstructure.

The phase structures were determined by X-ray diffrac-

*Corresponding author. Fax: +86-25-332 6028; e-mail: tangw@netra.nju.edu.cn

0925-8388/98/$ – see front matter
PII: S0925-8388(98)00771-3

tion (XRD) with Cu Kα radiation. The composition was determined using a scanning electron microscope equipped with an energy dispersive X-ray analysis (EDAX) unit. The crystallization temperature was determined by differential thermal analysis. The room-temperature magnetic properties were measured using a vibrating sample magnetometer with a maximum applied field of 2.0 T. The microstructures were studied by transmission electron microscopy (TEM).

3. Results and discussion

3.1. Formation and structure of $Sm_2(Fe,Al,Zr)_{17}C_{1.5}$ alloys

Figs. 1 and 2 show the XRD patterns for induction-melted $Sm_2Fe_{(15.5-x)}Zr_xAl_{1.5}C_{1.5}$ alloys and annealed $Sm_2Fe_{(15.5-x)}Zr_xAl_{1.5}C_{1.5}$ ribbons, respectively. It can be seen that both the induction-melted alloys and the annealed ribbons consist similarly of a multiphase structure. Besides the 2:17 phase with the rhombohedral Th_2Zn_{17}-type structure and α-Fe, a new phase is observed in the Zr-containing samples. The XRD results identify the new phase as ZrC with a cubic structure. Its lattice parameter and melting point are 0.4894 nm and 3540°C, respectively. With increasing Zr content, the amount of ZrC increases considerably and that of α-Fe decreases. This implies that the addition of Zr inhibits the formation of the α-Fe phase.

Because of a small excess of Sm compared to the 2:17 stoichiometry the induction-melted samples also contain $SmFe_2$ as an impurity phase. However, after the samples are quenched and then annealed, the $SmFe_2$ phase disappears, indicating a non-equilibrium nature of the rapid quenching process. According to the samarium–iron phase diagram, the $SmFe_2$ phase is formed by a series of peritectic reactions from the liquid phase and α-Fe phase. In this case, the rapid quenching process can hinder the transformation from the high temperature peritectic phase Sm_2Fe_{17} to the intermediate phase $SmFe_3$ or the low temperature peritectic phase $SmFe_2$.

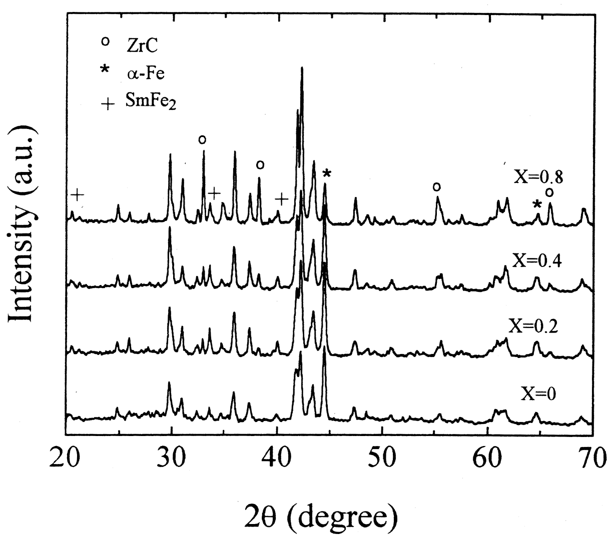

Fig. 1. XRD patterns of the as-cast $Sm_2Fe_{(15.5-x)}Zr_xAl_{1.5}C_{1.5}$ alloys.

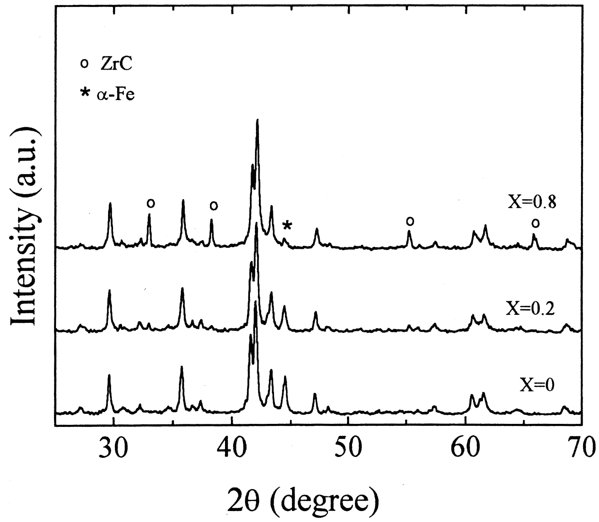

Fig. 2. XRD patterns of $Sm_2Fe_{(15.5-x)}Zr_xAl_{1.5}C_{1.5}$ ribbons annealed at 750°C for 30 min.

3.2. Crystallographic and intrinsic magnetic properties of induction-melted alloys

The crystallographic and intrinsic magnetic properties of the induction-melted alloys are summarized in Table 1. It can be seen that the lattice constants of the 2:17-type structure and the Curie temperature remain almost constant with Zr addition, which suggests that few Zr atoms substitute into the Sm or Fe sites. However, the room-temperature saturation magnetization M_s decreases monotonically with increasing Zr content from 104.6 emu g^{-1} for $x=0$ to 88.9 emu g^{-1} for $x=0.8$. As a result of the formation of ZrC, the interstitial C atoms are partially removed from the 2:17 phase. However, the saturation magnetization M_s and magnetic anisotropy field H_a are directly related to the introduction of C atoms and decrease with decreasing C atoms [8]. Additionally, the formation of ZrC reduces the fraction of magnetic phases in the alloys. Thus, this decrease in M_s may be attributed to both the effect of the non-magnetic ZrC phase and the reduction of the M_s for the 2:17 phase.

Table 1
Effects of Zr content on the crystallographic parameters and magnetic properties of $Sm_2Fe_{(15.5-x)}Zr_xAl_{1.5}C_{1.5}$ alloys

Zr content (x)	a (nm)	c (nm)	T_C (°C)	M_s (emu g^{-1})
0	0.8640	1.2504	215	104.6
0.2	0.8639	1.2506	220	97.0
0.4	0.8638	1.2505	220	94.9
0.8	0.8639	1.2507	220	89.0

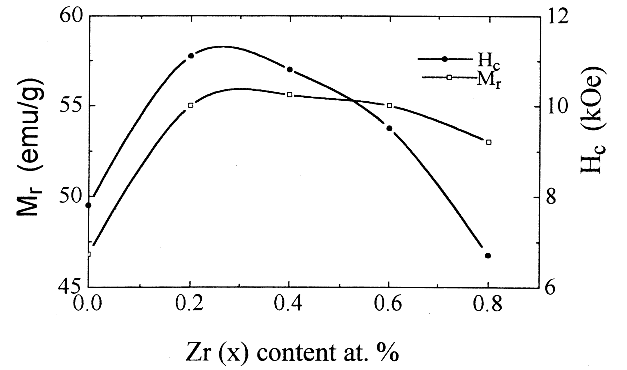

Fig. 3. Effect of Zr content on the magnetic properties of annealed $Sm_2Fe_{(15.5-x)}Zr_xAl_{1.5}C_{1.5}$.

3.3. Magnetic hardening and properties of annealed ribbons

The magnetic hardening of the induction-melted alloys for various Zr contents is completed using the melt-spinning technique. The as-spun ribbons have a very low coercivity due to the presence of an amorphous phase, which is determined by the XRD results. The high coercivity is developed by annealing the ribbons at 750°C, which is above the crystallization temperature determined by differential thermal analysis. Fig. 3 shows the effect of Zr content on the remanence M_r and coercivity H_c of the ribbons with various compositions. Initially, M_r and H_c increase rapidly with increasing Zr content, reaching an optimum value around $x=0.2$–0.4, and then decrease. As described above, the fraction of the non-magnetic ZrC phase increases at the expense of reducing the magnetic phase; the formation of the ZrC phase leads to decreasing M_s and H_a of the 2:17 phase. Thus, the excessive addition of Zr deteriorates both the remanence and coercivity.

The effect of the annealing time on M_r and H_c of the $Sm_2Fe_{(15.5-x)}Zr_xAl_{1.5}C_{1.5}$ ribbons with $x=0$ and 0.2 was also investigated and the results are shown in Fig. 4. As can be seen, M_r and H_c of the Zr-containing ribbon are not very sensitive to the annealing time compared to those for the Zr-free ribbon. This indicates that the addition of Zr helps to stabilize the microstructure of the ribbons during annealing. Spun at 40 m s^{-1} and then annealed at 750°C for 30 min, the $Sm_2Fe_{(15.5-x)}Zr_xAl_{1.5}C_{1.5}$ ribbon with $x=0.2$ obtains an optimum coercivity of up to 11.6 kOe together with a remanence of up to 55 emu g^{-1}. As expected for isotropic uniaxial magnetic ribbons, the optimum remanence is greater than $M_H/2$ (see Fig. 5; M_H is the magnetization measured at the maximum applied field of 2.0 T). This indicates that some α-Fe phase may be magnetically coupled to the 2:17 hard magnetic phase and thus the remanence is enhanced above $M_H/2$. Fig. 5 shows the corresponding hysteresis loops. We notice that the hysteresis loop of the Zr-free ribbon exhibits a step in the demagnetization curve. This characteristic could be caused by the presence of the coarse-grained α-Fe phase which leads to a weak exchange coupling to the hard magnetic phase. Compared with the Zr-free ribbon, the Zr-containing ribbon gives rise to a smooth demagnetization curve, which exhibits good squareness in the second quadrant. These results reveal that there exists a significant exchange coupling at the interphase boundaries. In this case, both the hard and soft regions reverse in unison to produce a smooth hysteresis loop with a higher remanence.

3.4. Microstructural changes

Fig. 6 shows typical TEM micrographs of annealed $Sm_2Fe_{(15.5-x)}Zr_xAl_{1.5}C_{1.5}$ ribbons with $x=0$ and 0.2. These images show the presence of a nanoscale mixture of the 2:17-type and α-Fe phases. However, an obvious difference in grain size is observed between the ribbon with and without Zr addition. The average grain size is determined to be 35 nm for the Zr-containing ribbon and 85 nm for the Zr-free ribbon. This observation indicates that Zr addition is effective in inhibiting grain growth during annealing. Unfortunately, the ZrC phase cannot be

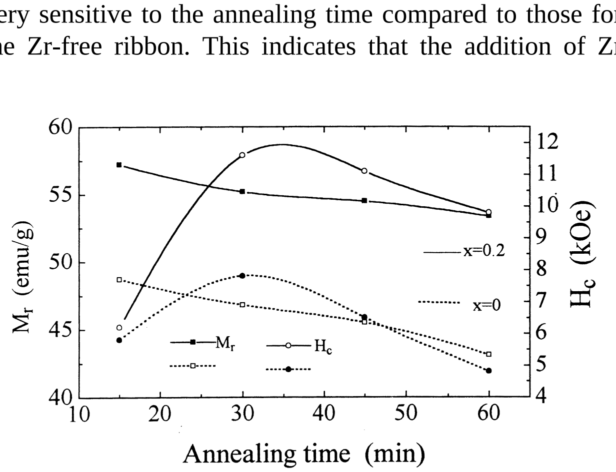

Fig. 4. Effect of annealing time on the magnetic properties of $Sm_2Fe_{(15.5-x)}Zr_xAl_{1.5}C_{1.5}$ ribbons.

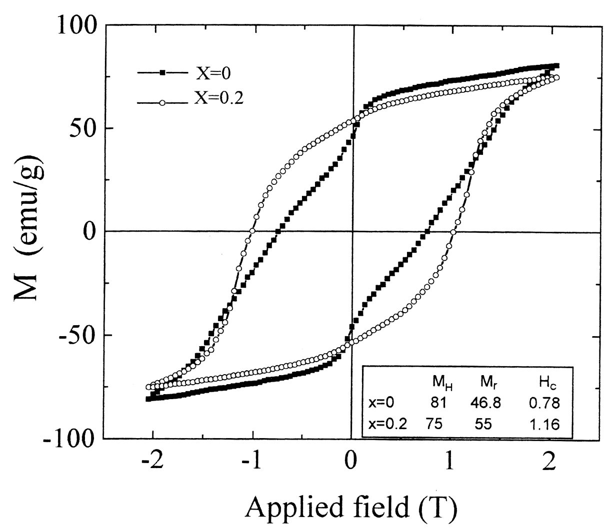

Fig. 5. Room-temperature hysteresis loops of $Sm_2Fe_{(15.5-x)}Zr_xAl_{1.5}C_{1.5}$ ribbons annealed at 750°C for 30 min.

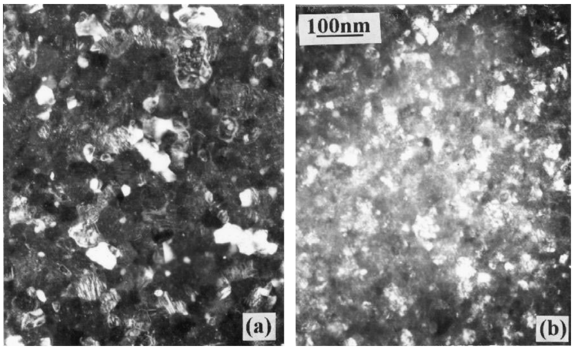

Fig. 6. Dark-field micrographs of $Sm_2Fe_{(15.5-x)}Zr_xAl_{1.5}C_{1.5}$ ribbons annealed at 750°C for 30 min. (a) $x=0$, (b) $x=0.2$.

distinguished in the TEM image of the Zr-containing ribbon. However, EDAX analysis for the induction-melted samples with $x=0.2$ reveals that the Zr distribution in the matrix and at the intergranular region is 0.05 and 2.36 at.%, respectively. Therefore, we conclude that ZrC appears mainly in the form of small precipitates within the intergranular regions.

The suppression of grain growth for the Zr-containing ribbons during annealing is directly related to the existence of the ZrC particles. The diffuse particles distributed around the grain boundaries can effectively limit the migration of grain boundaries and thus the grain growth. A mixture of fine-grained hard and soft magnetic phases is thought to prompt exchange coupling at interphase boundaries [9] and thus enhance the remanence. Moreover, the higher coercivity also results from these refined microstructures and can be explained by a simulation [10]. As a result, the addition of Zr to $Sm_2Fe_{(15.5-x)}Zr_xAl_{1.5}C_{1.5}$ is very effective at refining the grain size and enhancing exchange coupling at the interphase boundaries.

4. Conclusions

(1) The addition of Zr to $Sm_2Fe_{(15.5-x)}Zr_xAl_{1.5}C_{1.5}$ alloys results in the formation of a new phase, ZrC, within the intergranular regions. The formation of ZrC can effectively inhibit grain growth and eliminate free iron dendrites.

(2) The Curie temperature and crystallographic parameters remain almost constant with Zr addition, but the saturation magnetization decreases with increasing Zr content.

(3) An optimum coercivity of up to 11.6 kOe together with a remanence of up to 55 emu g^{-1} are obtained for the $Sm_2Fe_{15.3}Zr_{0.2}Al_{1.5}C_{1.5}$ ribbon annealed at 750°C for 30 min. The hysteresis loop of the ribbon displays a smooth demagnetization curve with better squareness. The high coercivity and remanence obtained in this study may be attributed to the addition of Zr, which leads to a fine-grained structure and significant exchange coupling between the hard and soft magnetic phases.

Acknowledgements

This work was supported by grant projects NMS and NSFC, and Province Jiang Su under contract No. BJ97043, People's Republic of China.

References

[1] B.G. Shen, L.S. Kong, F.W. Fang, L. Cao, J. Appl. Phys. 75 (1994) 6253.
[2] Z.H. Cheng, B.G. Shen, F.W. Wang, J.X. Zhang, J. Phys.: Condensed Matter 6 (1994) L185.
[3] S. Sugimoto, K. Kurihara, H. Nakamura, M. Okda, M. Homma, Mater. Trans. JIM 33 (1992) 146.
[4] Y.H. Zheng, A.S. Murthy, F.M. Yang, G.C. Hadjipanayis, J. Magn. Magn. Mater. 140–144 (1995) 1081.
[5] G.C. Hadjipanayis, Y.H. Zheng, A.S. Murthy, W. Gong, F.M. Yang, J. Alloys Comp. 222 (1995) 49.
[6] L.S. Kong, B.G. Shen, F.W. Wang, L. Cao, H.Q. Guo, T.S. Ning, J. Appl. Phys. 75 (1994) 6250.
[7] W. Tang, Z.Q. Jin, J.R. Zhang, S.Y. Zhang, Y.W. Du, J. Appl. Phys. 82 (9) (1997).
[8] H. Horiuchi, U. Koike, H. Kaneko, T. Kurino, H. Uchida, J. Alloys Comp. 222 (1995) 131.
[9] F.E. Pinkerton, C.D. Fuerst, Appl. Phys. Lett. 60 (1992) 2558.
[10] T. Schrefl, R. Fischer, J. Fidler, H. Kronmüller, J. Appl. Phys. 76 (1994) 7053.